Key role of the wetting layer in revealing the hidden path of Ge/Si(001) Stranski-Krastanow growth onset

Moritz Brehm,[1,*] Francesco Montalenti,[2] Martyna Grydlik,[1] Guglielmo Vastola,[2] Herbert Lichtenberger,[1] Nina Hrauda,[1] Matthew J. Beck,[3] Thomas Fromherz,[1] Friedrich Schäffler,[1] Leo Miglio,[2] and Günther Bauer[1]

[1]*Institute of Semiconductor and Solid State Physics, Johannes Kepler University, A-4040 Linz, Austria*
[2]*L-NESS and Materials Science Department, University of Milano–Bicocca, I-20125 Milano, Italy*
[3]*Department of Physics and Astronomy, Vanderbilt University, Nashville, Tennessee 37235, USA*

The commonly accepted Stranski-Krastanow model, according to which island formation occurs on top of a wetting layer (WL) of a certain thickness, predicts for the morphological evolution an increasing island aspect ratio with volume. We report on an apparent violation of this thermodynamic understanding of island growth with deposition. In order to investigate the actual onset of three-dimensional islanding and the critical WL thickness in the Ge/Si(001) system, a key issue is controlling the Ge deposition with extremely high resolution [0.025 monolayer (ML)]. Atomic force microscopy and photoluminescence measurements on samples covering the deposition range 1.75–6.1 ML, taken along a Ge deposition gradient on 4 in. Si substrates and at different growth temperatures (T_g), surprisingly reveal that for $T_g > 675\ ^\circ$C steeper multifaceted domes apparently nucleate *prior* to shallow {105}-faceted pyramids, in a narrow commonly overlooked deposition range. The puzzling experimental findings are explained by a quantitative modeling of the total energy with deposition. We accurately matched *ab initio* calculations of layer and surface energies to finite-element method simulations of the elastic energy in islands, in order to compare the thermodynamic stability of different island shapes with respect to an increasing WL thickness. Close agreement between modeling and experiments is found, pointing out that the sizeable progressive lowering of the surface energy in the first few MLs of the WL reverts the common understanding of the SK growth onset. Strong similarities between islanding in SiGe and III/V systems are highlighted.

PACS number(s): 81.07.Ta, 68.35.Md, 81.15.Hi

I. INTRODUCTION

The morphological evolution of the heterosystem Ge on Si(001) as a function of deposition Θ_{Ge} has been extensively studied in the last ten years,[1–3] as a prototype of the intriguing Stranski-Krastanow (SK) growth modality, where strain-driven evolution from a two-dimensional (2D) wetting layer (WL) to self-assembled three-dimensional (3D) islands is observed.[4,5]

The experiments carried out so far demonstrated a variety of possible island morphologies of different height-to-base aspect ratio (ar): prepyramids or mounds (ar<0.1),[6,7] shallow pyramids (ar=0.1) or rectangular huts bounded by {105} facets,[5,8] dome-shaped multifaceted islands (ar=0.22 –0.26),[5,9] or even steeper (ar=0.26–0.32) barn-shaped morphologies.[10] A simple explanation for this sequence of island shapes, which involves a progressive increase in the ar, occurring with increasing island volume V, can be offered by comparing the energy of an island with that of the WL. Elastic relaxation caused by the 3D geometry scales with V while the energy cost for exposing an extra surface grows with $V^{2/3}$, dominating in the small-volume limit, and therefore favoring shallow islands. As the island volume grows the volumetric term becomes more and more important and steeper islands appear, relaxing more effectively the elastic energy.[11] This description oversimplifies the processes which take place in real systems. The tendency toward higher island aspect ratios is counterbalanced by competing effects. It is well known that temperature-dependent SiGe alloying takes place in the islands and deep trench formation occurs[12]

around steep islands providing a simple kinetic path for Si spill out from the substrate. Since alloying lowers the effective misfit between island and substrate, this process decreases the volumetric term, thus allowing shallow islands to be stable even at larger volumes.[13] Moreover, islands were observed to undergo plastic relaxation,[14] causing a peculiar cyclic-growth mode.[15] Even neglecting the above effects, valid close to the onset of SK growth where intermixing is limited and island volumes are too small for dislocation nucleation, island stability is not determined solely by the volume. Indeed, it has been shown that the energetics of the WL is strongly thickness dependent up to a Ge coverage (Θ_{Ge}) of 4–5 ML.[16–18] Thus, in this range of Θ_{Ge} the appearance of stable islands is expected to critically depend on both, the volume *as well as* on the WL thickness.

In this paper we quantitatively analyze this issue by presenting a joint experimental and theoretical investigation of the onset of SK growth in Ge/Si(001). Particular care is dedicated to controlling the Ge deposition (reaching up to 0.025 MLs in resolution), unrolling and freezing the usual growth evolution along a space scale, i.e., obtaining an accurate deposition gradient across the wafer size (similarly to Ref. 19 where the onset of SK growth in InGaAs/GaAs(001) is investigated), and in measuring *on fly*, still *ex situ*, the WL thickness by photoluminescence (PL). From the theoretical point of view, *ab initio* calculations of layer and surface energies are suitably matched to finite element method (FEM) simulations of the elastic energy in islands, allowing for the comparison of the thermodynamic stability of different shapes with respect to an increasing WL thickness. We show

how the close matching between experiments, predictions, and guided experimental checks allows to discover a new hidden path in the morphological evolution of Ge on Si(001) islands, which clarifies the experimental scenario with temperature and modifies the current interpretation of it.

The paper is organized as follows. In Sec. II details of the sample-growth procedure, allowing a careful control of Θ_{Ge}, are given. Results of photoluminescence investigations to monitor the WL thickness, the onset of island formation and the transfer of material from the WL to the islands are presented. In Sec. III, the thermodynamic model is described that is used to understand the experimental evidence. It is shown that the model predicts a change in the relative stability of pyramids, domes, and WL as a function of the WL thickness, in excellent agreement with the experimental observations. A further set of experiments, aimed at better checking the model predictive power is reported in Sec. IV. In Sec. V the conclusions are presented.

II. EXPERIMENTS: GROWTH, PHOTOLUMINESCENCE, AND AFM

The samples were grown by solid source molecular-beam epitaxy (MBE) on high-resistivity 4 in. Si(001) wafers. After *in situ* oxide desorption at 1035 °C for 5 min, a 45-nm-thick Si buffer layer was grown at temperatures ranging between 550 and 700 °C. No influence of this temperature variation on the subsequent Ge deposition is observed. To achieve a shallow gradient of the impinging Ge flux across the wafer, the substrate rotation was turned off during Ge deposition. The variation in Θ_{Ge} across the wafer, which was determined by x-ray diffraction on thick pseudomorphic SiGe reference samples, resulted to $\pm 15\%$ with respect to the nominal value at the wafer center. Ge was deposited at a nominal rate of $R_{Ge}=0.05$ Å/s for most samples and at $R_{Ge}=0.01$ Å/s for reference samples. Seven growth series were investigated with deposition temperatures varied in between 612 and 750 °C. For PL investigations some of the wafers were capped with 50 nm of Si at low enough temperature (300 °C) to avoid intermixing, segregation, and shape transformations during capping.[20] The capless reference wafers were used for a quantitative evaluation of the shapes, densities, and volumes of the self-assembled Ge islands by atomic force microscopy (AFM). AFM and low-temperature (4.2 K) PL measurements were performed along the Ge thickness gradient on up to 90 positions across each wafer, leading to a Θ_{Ge} resolution of 0.025 ML. Both AFM and PL experiments were performed on more than 600 measurement points on a total of 21 wafers.

In the following, data are shown for growth at 700 and 625 °C, which represent two characteristic situations for Ge island formation. Figures 1(a)–1(d) show AFM inclination images of samples with $4.32 < \Theta_{Ge} < 4.95$ ML grown at $T_g = 700$ °C. Below $\Theta_{Ge} = 4.2$ ML no islands are observed whereas in the very narrow range from 4.32 to 4.35 ML only domes are observed with progressively increasing number. The inset of Fig. 1(a) shows a 3D image of a typical dome at a magnified scale (diameter 120 nm and height 22 nm). Only for $\Theta_{Ge} \geq 4.38$ ML large {105}-faceted pyramids with sizes
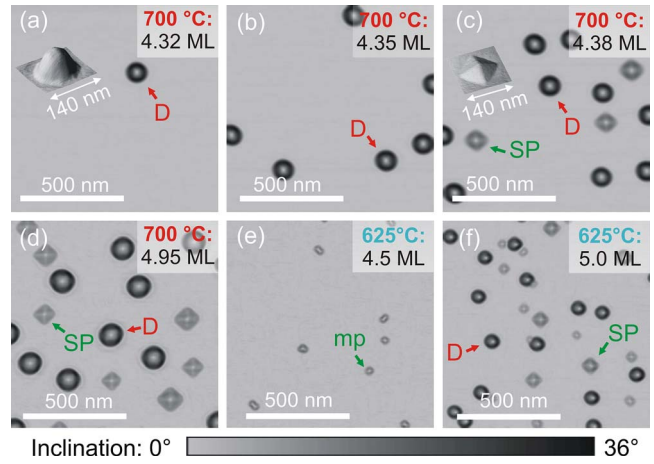

FIG. 1. (Color online) Inclination-angle AFM images displaying the local surface slope with respect to the (001) surface. (a)–(d) Evolution of Ge islands for $T_g = 700$ °C. Domes (*D*) appear prior to square based, large pyramids (SP). The insets in (a) and (c) show 3D AFM images of a typical dome and a pyramid. [(e) and (f)]: $T_g = 625$ °C. Up to $\Theta_{Ge} \approx 4.9$ ML only small, mp are observed; domes appear in addition for $\Theta_{Ge} > 4.9$ ML.

comparable to that of the domes [base diagonal of 120 nm, see Fig. 1(c) and magnified inset] are observed together with transition domes. Further increasing of Θ_{Ge} above ≈ 4.4 ML results in the additional nucleation of smaller pyramids (denoted as SP) with minimum base lengths of 60 nm, as shown in Fig. 1(d). In contrast to the pyramids, all domes in the Ge deposition range reported in Fig. 1 have virtually the same size.

The analysis of the AFM data was performed in the following way: for the detection of island shapes 1.5×1.5 μm^2 micrographs of the sample surface morphologies were recorded, for the determination of the island densities 5×5 μm^2 micrographs were analyzed, for the determination of the island volumes a combined analysis of the smaller and larger area scans was used. In order to demonstrate this analysis, in Fig. 2 micrographs (1.5×1.5 μm^2) of the sample surface morphology for different Θ_{Ge} are shown for $T_g = 700$ °C. Similar data were taken for all other growth
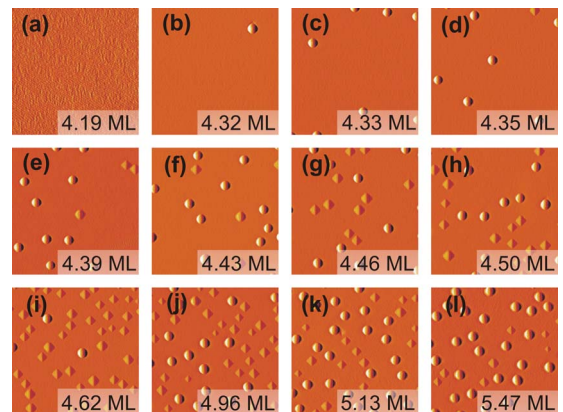

FIG. 2. (Color online) 1.5×1.5 μm^2 AFM scans in derivative mode. Evolution of the island morphology for $T_g = 700$ °C. The Ge coverage Θ_{Ge} is indicated by the labels of panels (a)–(l).
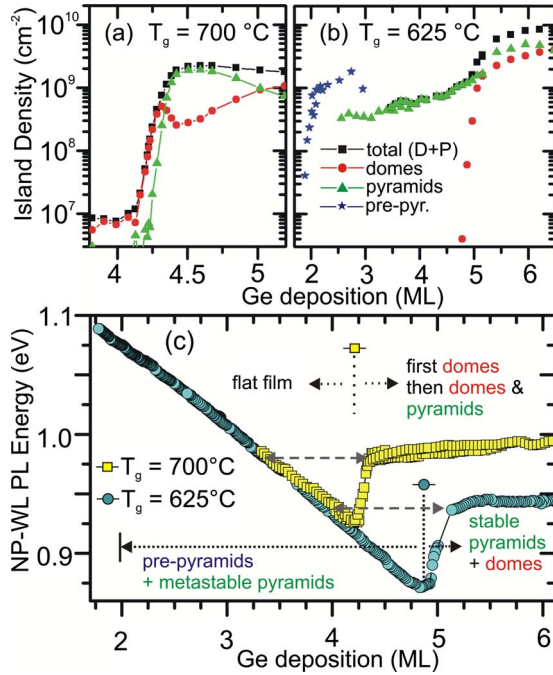
FIG. 3. (Color online) (a) and (b): Island density vs T_{Ge} at $R_{Ge}=0.05$ Å/s. At $T_g=700$ °C (a) domes form prior to pyramids. At $T_g=625$ °C (b) pre-pyramids (at $T_{Ge}\approx2$ ML) and metastable pyramids (at $T_{Ge}\approx2.5$ ML) are formed prior to domes (at $T_{Ge}\approx4.9$ ML). (c) NP-WL photoluminescence transition energy for $T_g=700$ °C (squares) and 625 °C (circles). An abrupt blue shift of the WL signal occurs at the onset of dome formation originating from a transfer of $T_{Ge}\approx0.93$ ML Ge from the WL to the islands.

temperatures and in Fig. 3 the analysis of the island densities is presented for two characteristic temperatures, namely, T_g =700 °C [Fig. 3(a)] and T_g=625 °C [Fig. 3(b)].

In Fig. 3(a) the evolution of the island population at T_g =700 °C is shown for $3.5<\Theta_{Ge}<5.5$ ML. No islands are observed for $\Theta_{Ge}<4.2$ ML (see also Fig. 2) whereas just domes appear at the onset of islanding. As soon as transition domes and large pyramids are observed, the density of domes decreases, from 5×10^8 to 2.4×10^8 cm^{-2}. Small pyramids nucleate at a coverage $\Theta_{Ge}>4.5$ ML [see Figs. 2(h)–2(l)]. With further Ge deposition (>4.6 ML) the density of domes increases on cost of the density of pyramids, with the total island density remaining constant.

At T_g=625 °C we do observe small prepyramids already above $\Theta_{Ge}\approx2$ ML [Figs. 3(b) and 6(a)], and {105}-faceted pyramids only from $\Theta_{Ge}\approx2.5$ ML up to $\Theta_{Ge}\approx4.9$ ML [Figs. 3(b), 6(c), and 1(e)], when the first domes appear. Between 2 and 4.6 ML the pyramid's average base length slightly increases from 29 to 39 nm whereas immediately after the dome onset [see Fig. 1(f)] some pyramids as large as 72 nm appear. In contrast to growth at 700 °C, the pyramid density increases monotonically throughout the deposition range investigated [see Fig. 3(b)].

By further varying T_g it was found that for all samples grown at $T_g>675$ °C domes nucleate prior to pyramids whereas for $T_g<675$ °C pyramids nucleate prior to domes.

To gain further insight into these unexpected observations, the WL thickness was characterized with high accu-
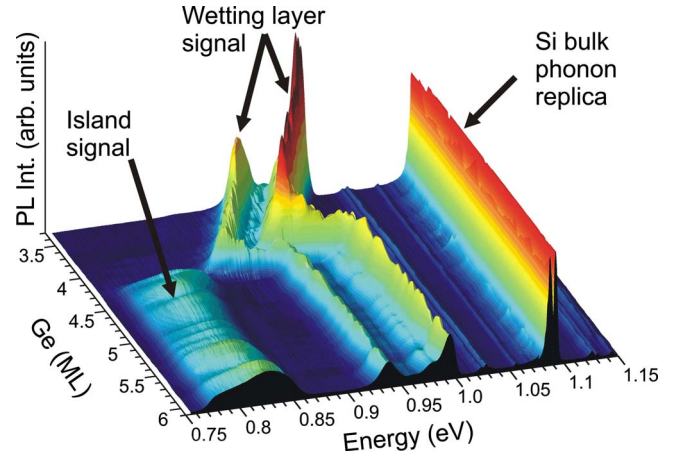

FIG. 4. (Color online) Three-dimensional plot of the PL spectra as a function of the Ge coverage for $T_g=700$ °C.

racy via confinement shifts in PL measurements.[21] In Fig. 3(c) the shift of the no-phonon (NP) WL transition energy is plotted versus Θ_{Ge} for $T_g=625$ and 700 °C. The shift of the WL transition energy between 3 and 4.2 ML for T_g =700 °C [Fig. 3(b)] was used in Ref. 21 to derive quantitative Ge profiles in the WL, which resulted in a maximum Ge content of $\approx85\%$. When the domes appear (4.25 ML at T_g =700 °C and 4.92 ML at T_g=625 °C) we see an abrupt blueshift of the WL PL signal by 0.06 eV (Figs. 3 and 4), which corresponds to the equivalent of 0.93 ML of the WL being transferred into the domes. Such a shift of the PL signal upon island nucleation was already reported in Refs. 22 and 23 but the much lower Θ_{Ge} resolution of these experiments did not allow a quantitative determination of the amount of transferred material.

In Fig. 4 a three-dimensional contour plot containing PL spectra measured for various Θ_{Ge} is shown for the range of $3.3<\Theta_{Ge}<6.1$ ML. The spectra are normalized to the dominating Si bulk PL emission at 1.095 eV (Ref. 24). Additionally to the properties of the WL PL as described in this Sec. II, Fig. 4 shows clearly that the appearance of the island PL (at 830 meV—indicating island nucleation) occurs concomitant with the WL thinning, evidenced by the abrupt blueshift of the WL related PL signal. After the onset of dome nucleation both the WL and the island emission bands remain almost at constant energy in the experimentally recorded Θ_{Ge} range. The individually recorded PL line scans can be extracted from movie 1 (see Ref. 25).

III. MODELING

To understand which types of islands are thermodynamically stable and which are observed because of kinetic effects, modeling based on quantitative data was performed. Considering a Ge WL with a thickness of N monolayers (N-WL) on Si(001), the WL is subcritical with respect to island formation if additional Ge atoms have a lower energy in the $(N+1)$-WL compared to Ge atoms in a 3D island. The energy difference Δ between the 3D and the 2D (WL) configuration (just including the relevant volumetric and surface

contributions, see Appendix) can be written as

$$\Delta = V_{is}\rho_{is} - V_1\rho_{eff}(N+1) + S\gamma_{is} - A\gamma(N), \quad (1)$$

V_{is} and V_1 represent the volumes occupied by the n_{at} atoms in the island configuration or in the additional flat layer,[26] respectively, ρ_{is} is the elastic-energy density in the island (including the substrate deformation), γ_{is} is the average surface energy of the island facets, S is the area of the exposed facets, A is the WL area covered by the island, and $\gamma(N)$ is the surface energy of the N-WL. $\rho_{eff}(N+1)$ is the energy density with respect to Ge bulk of the additional layer, including ρ^t, the energy density of tetragonally strained bulk Ge, and the variations in surface energy γ due to replacement of the Nth layer with the $(N+1$st) one, both of thickness h_1,

$$\rho_{eff}(N+1) = \rho^t + \frac{1}{h_1}[\gamma(N+1) - \gamma(N)]. \quad (2)$$

This dependence of ρ_{eff} on N, already pointed out in Refs. 16–18, turns out to be crucial in establishing the stability of different island shapes with respect to the WL. Recent calculations have shown that $\gamma(N)$ decreases with N for typical low-energy Ge/Si(001) reconstructions,[17,18] reaching its limiting value for N at about 5[18,27] (a similar trend takes place also in the InGaAs/GaAs(001) system,[28] where, however, a limiting value is reached for a much smaller WL thickness). In order to obtain quantitative estimates of Δ, we used an approach similar to Ref. 29, i.e., we exploited density-functional theory (DFT)-derived surface energies (when available from the literature) while ρ_{is} for pyramids and domes was evaluated by continuum elasticity theory, using a FEM solver. As pointed out in Appendix, particular care was dedicated to ensure consistence of FEM and DFT, using elastic constants based on DFT calculations, also exploited to add nonlinear corrections to the elastic energy. Furthermore, $\gamma(N)$ was taken from the DFT calculations of Ref. 18, where a (2×8) reconstruction is considered, after subtracting the very small Ge/Si interfacial energy (≈ 1 meV/Å^2, see Ref. 17). The surface energy of the pyramids (γ_{pyr}) was also derived from Ref. 18. This required integrating the strain-dependent values for the {105} surface in Ref. 18 (see also Refs. 30 and 31 for a further characterization of such a surface) over the top-down increasing strain field at the free facets, as computed by FEM, yielding an average, size-independent value of $\gamma_{pyr}=59.8$ meV/Å^2. The surface energy of the multifaceted dome, γ_{dome}, cannot be estimated because of the unknown values for some facets. We therefore used a reasonable $\gamma_{dome}=65$ meV/Å^2 and verified that variations in γ_{dome} in the range between 61 and 69 meV/Å^2 do not alter our findings. More details on the set of employed parameters and on their influence on the model outcome can be found in Appendix, where some general limitations of Eq. (1) are also discussed. Before presenting the quantitative results for Δ as a function of shape, volume, and WL thickness, it is worth considering some general features of Eq. (1). If the film is sufficiently thick so that the WL surface energy does not depend on N anymore, then the volumetric term in Eq. (1) reduces to $V(\rho_{is}-\rho^t)$. Since the presence of inclined facets allows the system to relax part of the elastic energy,
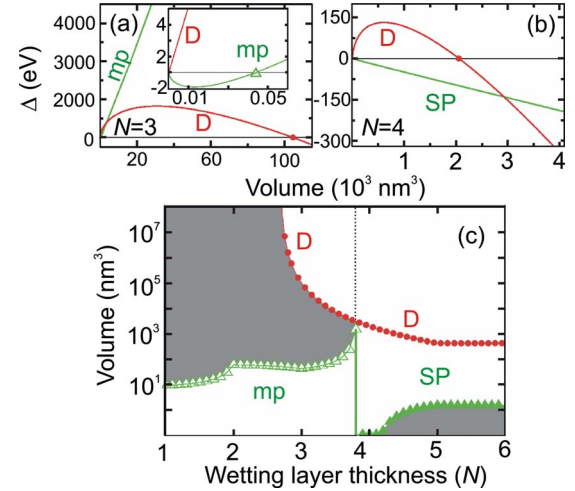

FIG. 5. (Color online) (a) and (b): calculated energy difference $\Delta(V)$ of pyramids and domes with respect to the flat WL. (a) At $N=3$ the pyramids (green, mp) are not stable except for very small volumes (inset). (b) At $N=4$ pyramids (SP) are more stable than the WL for any volume. At both thicknesses, instead, domes (red, *D*) display the usual nucleation behavior. (c) Critical island volumes vs WL thickness. Gray regions indicate areas where no islands can exist. For $N<3.8$ mp pyramids can only exist up to the maximum volume indicated by empty triangles. For $N\geq 3.8$ [$N_c(P)$ in the text], pyramids (SP curve) are more stable than the WL above a minimum (negligible) volume indicated by full triangles. Domes are stable for $N\geq 2.7$ [$N_c(D)$ in the text] and then only above the critical volume indicated by full circles.

this term is negative; in this limit there always exist a finite critical volume (quantitatively determined also by surface terms) beyond which islands are favored with respect to the 2D configuration. For small enough N, instead, the progressive lowering (with increasing N) of the WL surface energy introduces a driving force favoring the flat WL against island nucleation. The volumetric term in this case reads $V[\rho_{is}-\rho_{eff}(N+1)]$, with $\rho_{eff}(N+1)\leq \rho^t$ so that for a fixed N a finite critical volume can be associated only to those 3D islands able to offer sufficient elastic-energy relaxation. For thicknesses below 2 ML, however, the surface-energy effect is so strong that even complete elastic relaxation would not be sufficient to promote formation of stable islands.[17] In the following we present quantitative results, illustrating how the above considerations come into play. Figures 5(a) and 5(b) show the dependence of Δ vs V for pyramids and domes for two WL representative thicknesses. For $N=3$, the $\Delta(V)$ curve for domes follows the usual nucleation theory behavior. Beyond a critical volume, the formation of domes is increasingly favored against WL thickening, i.e., once formed, thermodynamics drives dome enlargement up to a maximum value, not addressed here.[32] From the same figure, it is evident that pyramids for $N=3$ are not stable, except at extremely small volumes of $V<50$ nm^3 [Fig. 5(a), inset], where the $\Delta(V)$ curve for pyramids has a minimum below the WL energy. At such small WL thicknesses volume enlargement of the pyramids is hindered because piling up Ge in the pyramids diminishes the influence of the strong binding of Ge close to the Si-Ge interface. This effect outweighs
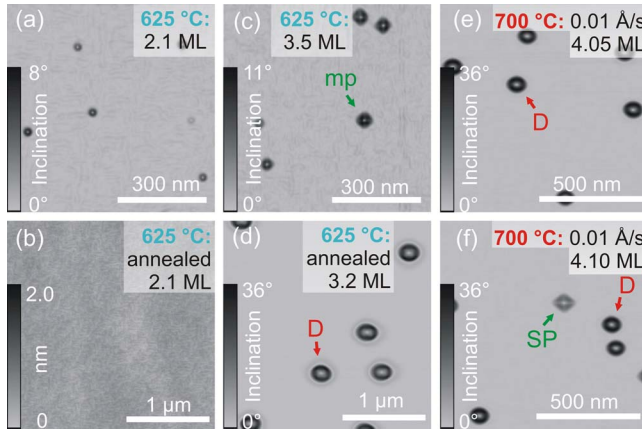
FIG. 6. (Color online) [(a), (c), and (d)]: AFM inclination images and (b) local height AFM image of Ge islands grown at T_g =625 °C. At 2.1 ML (a) small prepyramids (base length: 20 nm) are observed, at 3.5 ML (c): pyramids (base length up to 50 nm). Annealing of the samples in (a) and (c) for 160 min at 700 °C leads to flat film formation for $2.0 < \Theta_{Ge} < 3.2$ ML (b), and dome formation for $\Theta_{Ge} = 3.2$ ML (d). [(e) and (f)]: AFM inclination images, at $T_g = 700$ °C and $R_{Ge} = 0.01$ Å/s domes (D) are still formed prior to pyramids but already at $\Theta_{Ge} \approx 4.05$ ML. Note the different length scales.

the energy gain due to island strain relaxation and results in a positive volumetric term in Eq. (1). However, sufficiently small islands are stabilized by the large surface energy of the WL with respect to the one of {105} surfaces which at such small WL thicknesses compensates the positive volumetric contribution.

The actual stability of such small islands is, however, questionable (see Appendix) since the chemical potential at the minimum of the $\Delta(V)$ curve is equal to the one of the WL [Fig. 5(a), inset] and it is likely that at sufficiently high temperatures the metastable pyramids mp dissolve into the WL, for which further volumetric growth is not hindered. For $N = 4$ [Fig. 5(b)], the $\Delta(V)$ curve for the pyramids is lower in energy than that of the WL at any volume since both volumetric and surface contributions are negative (resulting in barrierless island formation) while the dome behavior remains qualitatively unchanged.

In Fig. 5(c) we display critical volumes [conventionally computed by imposing $\Delta(V) = 0$] for island appearance as a function of the WL thickness. In order to offer a continuous picture, Δ is plotted also for noninteger thickness. The Δ values for a monolayer coverage between N and $N + 1$ were computed by a simple linear interpolation of $\gamma(N)$ so that Δ represents the energy difference between the islands and the WL obtained by adding Ge to a flat film of N monolayers with a fraction of the surface covered by $(N + 1)$ ML terraces, neglecting the influence of step energies.

The possibility of obtaining highly nontrivial equilibrium phase diagrams in Stranski-Krastanow growth was already pointed out in Ref. 33. Figure 5(c) now demonstrates that for a realistically modeled Ge/Si(001) system, a complex behavior is indeed found. Our model predicts a minimum WL thickness $N_c(D) = 2.7$ for dome formation. Regarding pyramids, up to $N = 3.8$ metastability is found (mp curve in Fig.

5) while for $N > N_c(P) = 3.8$ also pyramids become stable (SP), starting from negligibly small critical volumes.

According to our thermodynamic calculations, hence, only from $N > N_c(D) = 2.7$ formation of stable domes is favored against the increase in the WL thickness. Moreover, there exists a range $N_c(D) < N < N_c(P)$, where domes are stable while pyramids are not. Finally, for $N > N_c(P)$ both pyramids and domes are more stable than the WL for sufficiently large volumes, pyramids being favored at small volumes due to the reduced surface-energy cost. This is the typical situation considered when such bimodal distributions are discussed in the literature.[5,34]

A thermodynamic analysis alone can help interpreting experiments but it is clear that a quantitative comparison would require a kinetic treatment, a daunting task considering the need of correctly describing the aforementioned WL surface-energy decrease with thickness, the influence of reconstruction, and atomic-scale diffusion mechanisms which are expected to be activated at the relatively high-growth temperatures. Some very general conclusions, however, can be drawn directly from Fig. 5(c). For $N = N_c(D)$ an infinite number of atoms should be collected in order to form a stable dome. At higher coverage, the critical volume decays, making dome formation possible. Hence, dome formation will always take place at some overcritical WL thicknesses. Always on very general grounds, we can state that higher atomic mean-free paths, determined by higher growth temperature (and/or lower deposition fluxes) allow for dome nucleation under less overcritical conditions. This is confirmed by the experimental observations (Fig. 1). Furthermore, Fig. 5(c) shows that if domes nucleate under overcritical conditions, thermodynamics allows for their enlargement at the expense of the WL. Indeed, as soon as, for a given $N > N_c(D)$, the dome volume exceeds the critical one, stability at a lower N is guaranteed; the WL thickness is reduced while the domes grow.[32] Notice that the WL thickness cannot be reduced below $N = N_c(D)$. These predictions are in excellent agreement with the experimental results reported in Sec. II [in particular, see the PL data of Figs. 3(c) and 4], showing an abrupt WL thinning (by ~1 ML) concomitant with (over-critical) dome formation.

A further understanding of the processes leading to dome formation requires more qualitative arguments; the main problem is in understanding how sufficient material can be collected and arranged into a dome shape. A large multifaceted structure is not likely to form directly from a 2D film. In fact, experiments have shown how domes can originate from pyramids, exploiting a complex shape transformation.[35,36] Even though domes become stable at lower WL thicknesses, pyramids are still needed as precursors to drive material to the dome shape. For $N < N_c(P)$, however, a forbidden gap in size [gray region in Fig. 5(c)] is present, separating the mp curve from the dome one. By growing the WL above the critical thickness for SP formation, pyramids can finally increase their volume and transform into domes. It is, however, possible to imagine dome formation also on a less overcritical WL; as N increases in the range $N_c(D) < N < N_c(P)$, indeed, the volume of mp grows progressively while the dome one decreases so that the volumetric gap diminishes. This increases the probability that, if sufficient thermal energy is

provided, fluctuating mps can collect a random flow of material from the surrounding area, providing the required additional volume even below the critical thickness for stable pyramid formation.

In Figs. 3(b) and 3(c) and Fig. 1(e) it is shown that pyramids appear prior to domes only at lower growth temperatures ($T_g < 675$ °C). Our interpretation based on Fig. 5(c) is that those pyramids are "frozen" mps. Being metastable and, as such, unable to grow above a certain size, they are quickly dissolved at higher growth temperatures, e.g., for $T_g = 700$ °C. So that when the first islands are observed, these are already domes, originated from a sudden transition from "fluctuating" mps [Figs. 1(a) and 1(b)]. Due to the high temperature, the process is so fast that only large enough, stable islands (domes) are seen. At high coverage, pyramids are predicted to become stable, and indeed both at high and low T_g the usual bimodal distribution[5,34] is eventually recovered. However, the sudden appearance of pyramids after domes at high T_g [Fig. 1(c)] is probably linked to a more complex effect. Indeed, Fig. 3(c) indicates that after dome formation the WL remains very thin even for further Ge deposition so that stable pyramids are not predicted based on Fig. 5(c). This apparent breakdown of the model predictions is not surprising; mature domes are well known to dig deep trenches around their periphery,[12] inducing island enrichment with Si, and therefore influencing the relative stability of islands vs WL. As already pointed out, our model does not consider the role played by SiGe alloying and cannot be directly used to infer the system behavior when intermixing is important. A suitable extension is left for future work.

We have shown that many of the data displayed in Figs. 1–4 can be interpreted based on the theoretical results of Fig. 5(c), however, the relative island stability as a function of the WL thickness was mainly inferred from theory alone. Therefore we designed an additional set of experiments aimed at a further proof of our interpretation, and at testing the model also from a more quantitative point of view.

IV. ANNEALING EXPERIMENTS AND MBE GROWTH WITH REDUCED GROWTH RATE

Small pyramids were clearly observed prior to domes in experiments at a growth temperature of $T_g = 625$ °C. According to the theoretical model presented in the previous Sec. III, such islands should be unstable since the limited strain release offered by these shallow structures is not sufficient, for WL thicknesses below 3.8 ML, to balance the effect of the decreasing WL surface energy.

To prove this interpretation, we annealed samples with mps grown at $T_g = 625$ °C for 160 min at 700 °C, in order to limit kinetic effects. The pyramids nucleated in between $2 \leq \Theta_{Ge} \leq 3.2$ ML evolved into a flat WL [Figs. 6(a) and 6(b)]; the ones for 3.2 ML $\leq \Theta_{Ge}$ generated only large domes [e.g, Figs. 6(c) and 6(d)]. These results are in semi-quantitative agreement with the predictions from Fig. 5(c) (flat film up to 2.7ML, domes above).

Moreover, if during deposition at $T_g = 700$ °C the Ge growth rate R_{Ge} is reduced from 0.05 to 0.01 Å/s, the onset of dome formation is shifted to lower coverage [Figs. 1(a)

and 6(e)] as predicted in Sec. III, since the increased ratio between surface diffusion length and deposition rate allows for a reduced overcriticality of the WL.

V. DISCUSSION AND CONCLUSIONS

In conclusion, exploiting a close comparison between experiments and theory, we have shown that at the very onset of 3D growth in Ge/Si(001) the WL thickness critically determines the shape of stable islands. The usual sequence flat film—pyramids—domes is thermodynamically justified only above 4 ML. On a thinner WL, instead, domes are stable islands, pyramids are not. Dome nucleation at temperature-dependent overcritical thicknesses, concomitant with a sudden WL thinning, was also demonstrated and theoretically justified.

Furthermore, we have clarified the important role of kinetics both, in (de)stabilizing small pyramids or in promoting their sudden transformation to domes.

Our results show that analogies between Ge/Si(001) and InGaAs/GaAs(001) are even stronger than previously realized.[37] The dependence of the WL surface energy (and thus, of the island stability) on the coverage, inducing a tendency toward nucleation at overcritical WL thicknesses followed by WL consumption, seems to be indeed quite similar in the two systems.[19,28,29,38]

APPENDIX: MODEL PARAMETERS

In order to minimize the number of free parameters, we used DFT whenever possible to evaluate the various terms of Eqs. (1) and (2). The elastic-energy density ρ_{is} in 3D islands, however, requires way too large simulation cells (particularly for the multifaceted dome shape) to be treated directly from first principles. We hence evaluated this term by continuum elasticity theory, using FEM. Also the strain tensor, used to establish the pyramid's surface energy (see Sec. III) was deduced from FEM calculations. All other terms, instead, were directly inferred by DFT (except for the dome surface energy, where DFT estimates were however used to establish, at least, typical values). As explained below, particular attention was dedicated to combine DFT- and FEM-derived estimates in a consistent way.

Quantum-mechanical calculations based on density-functional theory were performed using the VASP (Refs. 39–42) code and exploited to calculate relevant elastic constants. For all calculations, the electronic wave function was expanded in plane waves with kinetic energies up to 188 eV. Eigenvalues were calculated on a Monkhorst-Pack grid of special k points with a density of 8 points per reciprocal-lattice vector. Exchange and correlations were described by the Ceperley-Alder functional[43] as parametrized by Perdew and Zunger.[44] Pseudopotentials[45,46] were used to model the

TABLE I. Si and Ge elastic constants and lattice parameters as given by DFT.

	Silicon	Germanium
C_{11} (GPa)	160.2	121.6
C_{12} (GPa)	62.1	46.5
C_{44} (GPa)	76.2	64.3
Lattice constant (Å)	5.39	5.62

core electrons and the atomic nuclei, and periodic boundary conditions were employed. Bulk elastic constants for Si and Ge are reported in Table I and were calculated by applying small positive and negative strains along the distinct symmetry directions of the crystal.

Using DFT-computed elastic constants, FEM calculations were run on a flat Ge epilayer on a Si substrate for values of the in-plane Ge strain ranging from 0% to −6%, the elastic-energy density was extracted in meV/Å^3, where the volume of the deformed cubic unit cell was calculated using $V = V_0(1 + \mathrm{Tr}\,\varepsilon)$, and $\mathrm{Tr}\,\varepsilon$ denotes the trace of the strain tensor. DFT elastic energies were converted into meV/Å^3 using the DFT-computed volumes of strained cubic cells. FEM and DFT results were compared and a numerical correction factor f was extracted at each strain value to achieve FEM consistency with DFT calculations. These correction factors allow FEM to account for nonlinear terms in the elastic energy. The calculated correction factors are compiled in Table II and demonstrate that even for rather moderate strains occurring in the Ge on Si system, nonlinear corrections are not negligible. Quadratic interpolation was used to obtain the correction factor for any strain value between 0% and −6%. With this DFT-fitted correction function added to the FEM code, the elastic-energy densities calculated for actual Ge island shapes are consistent with *ab initio* calculations. In particular, FEM and *ab initio* calculations give exactly the same result for the elastic energy stored in a Ge epilayer biaxially strained to the Si bulk lattice parameter.

DFT-based corrections for nonlinear elasticity were implemented for Ge but not considered to be relevant for Si.

Strain primarily accumulates in the Ge island while the deformation in the Si substrate is much weaker.[47]

As already pointed out in Sec. III, each of the surface terms which appear in Eqs. (1) and (2) can be reliably estimated using published DFT calculations, with the exception of the dome surface energy. Since domes are characterized by multiple facets, {001},{105},{113}, and {15 3 23} (in our FEM calculations we used the realistic dome geometry described in Ref. 14), one could attempt to compute γ_{dome} by considering a suitable weighted average of the surface energies of the various reported facet orientations. Considering that both {001} and {105} facets are found close to the island top, where strain relaxation is strong, values of around 64–66 meV/Å^2 can be expected for these facets.[18] For the {113} surface, an estimate of about 62 meV/Å^2 was found by DFT for unstrained Ge(113).[48] However, the {15 3 23} surface was never analyzed by DFT because of the very large unit cell. While it is very likely that the high indexes lead to a large surface energy, quantitative estimates are difficult. From the above numbers, however, it seems appropriate to assume a value of around 63 meV/Å^2 as a reasonable lower limit. Results reported in the Sec. III were obtained by setting $\gamma_{dome} = 65$ meV/Å^2. We here assess the relevance of the exact value of γ_{dome} on the N-dependent critical volumes for dome nucleation by varying γ_{dome} in the range $61 < \gamma_{dome} < 69$ meV/Å^2. The results are shown in Fig. 7, where the same calculations leading to Fig. 5(c) are repeated within the aforementioned range of γ_{dome}.

First of all, we notice that the WL critical thickness for dome formation (2.7 ML) is not affected by γ_{dome}. As explained in Sec. III, this number is determined solely by the volumetric term. Also, the qualitative behavior of the curves for domes compared to the ones for the pyramids is unchanged: the existence of a volumetric gap between mp pyramids and domes persists down to $\gamma_{dome} = 61$ meV/Å^2, a value which is expected to underestimate the real surface energy. Since also the monotonous decrease in the critical dome volume with increasing WL thickness is preserved, we notice that all conclusions of Sec. III are virtually independent of the actual value used for γ_{dome}, provided that variations are allowed within a reasonable range of values.

TABLE II. From left to right, columns show the Ge lattice parameter a, the corresponding biaxial strain, its elastic-energy density W computed by DFT (per atom in column 3 and per volume in column 5, the conversion being based on the unit-cell volume, column 4). Later, ρ (column 6) is the elastic-energy density computed by FEM and the correction factor f, computed from columns 5 and 6, is shown in column 7.

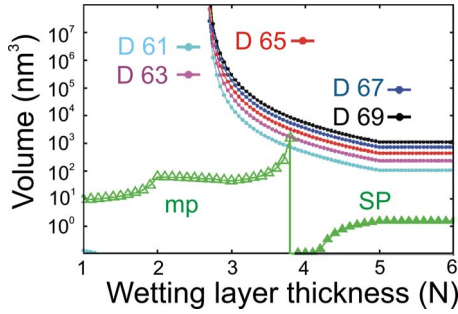|		DFT	DFT	DFT	FEM	f
a (Å)	strain	W (meV/atom)	Unit-cell volume (Å^3)	W (meV/Å^3)	ρ (meV/Å^3)	
5.625	0.00	0.000	179.343	0.000	0.000	1.000
5.569	−0.01	1.933	177.152	0.087	0.083	1.046
5.512	−0.02	7.872	174.895	0.362	0.339	1.065
5.456	−0.03	18.157	172.608	0.846	0.774	1.093
5.400	−0.04	32.918	170.340	1.554	1.394	1.115
5.344	−0.05	52.650	168.008	2.521	2.207	1.142
5.287	−0.06	77.594	165.715	3.766	3.220	1.169

FIG. 7. (Color online) Critical volumes vs WL thickness for different values of the dome surface energy (the number with the same color of the curve gives γ_{dome} in meV/Å^2). The pyramid curve (green) is exactly the one reported in Fig. 5(c). We recall that in the "mp" region the curve gives a maximum volume beyond which the WL becomes more stable than the *metastable* pyramids while in the "SP" one pyramids follow the usual nucleation theory and the curve indicates the volume above which pyramids become stable.

In the following, we discuss the dependence of island formation on the pyramid surface energy. Results in Fig. 5(c) were obtained using $\gamma_{pyr}=59.8$ meV/Å^2. This value was deduced from DFT calculations,[18] leading to (biaxial) strain-dependent values which we averaged over the pyramid facet after determining the position-dependent strain field by FEM. While this procedure appears to be solid[49] some error (DFT is not exact and the strain at the pyramid facet is not fully biaxial) must be expected. Here we test the dependence of our results on γ_{pyr} by attributing a reasonable uncertainty of 0.5 meV/Å^2. Results appear to change qualitatively, as shown in Fig. 8 where critical island volumes are computed using $\gamma_{dome}=65$ meV/Å^2 and varying γ_{pyr}. While for $\gamma_{pyr}=59.8$ meV/Å^2 or lower, the maximum pyramid volume in the mp region (empty triangles) grows with N, it is sufficient to increase γ_{pyr} by only 0.5 meV/Å^2 to observe vanishing critical volumes for a coverage between 3.5 and 3.9 ML. Notice that also the SP curve changes, becoming more similar to the one for domes (nucleation involving a barrier and critical volume decreasing with N). This nonmonotonous change in the model behavior is due to the almost degenerate values of the WL and of the {105} surface energies.[49] Very importantly, even if the difference between the curve for the highest surface energy (purple symbols) and the other ones seems to be very pronounced, the overall physical picture does not change considerably. If the smaller value of γ_{pyr} is considered, the role of mp as precursors, progressively (with increasing coverage) allowing to collect material sufficient to form stable domes, is reinforced. If, instead, the curve for the larger γ_{pyr} value is followed, then dome formation seems to be possible only after the critical thickness for stable pyra-
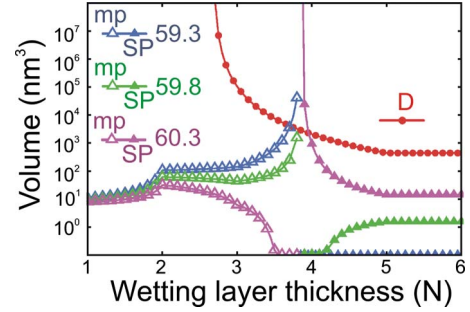

FIG. 8. (Color online) As in Fig. 7, but keeping fixed $\gamma_{dome}=65$ meV/Å^2, while considering three slightly different values of γ_{pyr}, given in meV/Å^2. Metastable pyramids (mp) are represented by empty triangles and stable pyramids (SP) by full triangles.

mid formation is reached since mp volumes are vanishing. Distinguishing which curve better describes the experimental results of Sec. II seems to be difficult. Even for vanishing mp volumes, pyramids could still be created (and appear in AFM images at low enough temperature), as a result of kinetic limitations inducing a sufficient lifetime even for structures less stable than the WL.

Summarizing the above observations, the presence of mp metastable volumes can help to reach the dome configuration by exploiting a local energy minimum. However, the experimental observations are consistent also with a model where pyramids are not even metastable at low coverage (below the onset of their SK behavior). This observation is important since the whole mp region is the one where reliable quantitative estimates of pyramid stability are more difficult to provide, not only due to the above discussed dependence of model results on γ_{pyr}. Equation (1), indeed, does not include $o(V^{2/3})$ terms (linked, e.g., to the presence of edges [1]). These terms do not play a role at "large" volumes [so that the critical thicknesses for dome and pyramids formation, $N_c(D)$ and $N_c(P)$, is unaffected] but they could influence quantitative estimates in the mp region. Notice that in the $V \rightarrow 0$ limit several other complications arise. For example, very small exposed facets could be only partially reconstructed. Also, in this limit, a non-negligible fraction of the atoms in the islands could still be influenced by the presence of the substrate, leading to a height-dependent chemical potential similar to the one characterizing WL atoms. All these aspects seem to require very complex modeling.

We conclude that there exist regions within the (N, V) space (the whole $V \rightarrow 0$ region and the region close to the mp-SP transition) where attempting to provide quantitative estimates is extremely speculative. However, these regions are not the ones which influence the main conclusions of our model, with respect to the stability of domes compared to the one of pyramids and of the tendency toward dome formation accompanied by WL thinning.

*moritz.brehm@jku.at

[1] V. A. Shchukin and D. Bimberg, Rev. Mod. Phys. **71**, 1125 (1999).

[2] J. Stangl, V. Holý, and G. Bauer, Rev. Mod. Phys. **76**, 725 (2004).

[3] I. Berbezier and A. Ronda, Surf. Sci. Rep. **64**, 47 (2009).

[4] J. V. Barth, G. Constantini, and K. Kern, Nature (London) **437**, 671 (2005).

[5] G. Medeiros-Ribeiro, A. M. Bratkovski, T. I. Kamins, D. A. A. Ohlberg, and R. S. Williams, Science **279**, 353 (1998).

[6] A. Vailionis, B. Cho, G. Glass, P. Desjardins, D. G. Cahill, and J. E. Greene, Phys. Rev. Lett. **85**, 3672 (2000).

[7] K. M. Chen, D. E. Jesson, S. J. Pennycook, T. Thundat, and R. J. Warmack, Phys. Rev. B **56**, R1700 (1997).

[8] Y.-W. Mo, D. E. Savage, B. S. Swartzentruber, and M. G. Lagally, Phys. Rev. Lett. **65**, 1020 (1990).

[9] J. A. Floro, E. Chason, L. B. Freund, R. D. Twesten, R. Q. Wang, and G. A. Lucadamo, Phys. Rev. B **59**, 1990 (1999).

[10] M. Stoffel, A. Rastelli, J. Tersoff, T. Merdzhanova, and O. G. Schmidt, Phys. Rev. B **74**, 155326 (2006).

[11] G. Vastola, R. Gatti, A. Marzegalli, F. Montalenti, and L. Miglio, in *Self-Assembled Quantum dots*, edited by Z. M. Wang (Springer, Berlin, 2008).

[12] S. A. Chaparro, Y. Zhang, and J. Drucker, Appl. Phys. Lett. **76**, 3534 (2000).

[13] M. De Seta, G. Capellini, F. Evangelisti, and C. Spinella, J. Appl. Phys. **92**, 614 (2002).

[14] A. Marzegalli, V. A. Zinovyev, F. Montalenti, A. Rastelli, M. Stoffel, T. Merdzhanova, O. G. Schmidt, and L. Miglio, Phys. Rev. Lett. **99**, 235505 (2007).

[15] F. K. LeGoues, M. C. Reuter, J. Tersoff, M. Hammar, and R. M. Tromp, Phys. Rev. Lett. **73**, 300 (1994).

[16] J. Tersoff, Phys. Rev. B **43**, 9377 (1991).

[17] M. J. Beck, C. Van de Walle, and M. Asta, Phys. Rev. B **70**, 205337 (2004).

[18] G. H. Lu, M. Cuma, and F. Liu, Phys. Rev. B **72**, 125415 (2005).

[19] F. Arciprete, E. Placidi, V. Sessi, M. Fanfoni, F. Patella, and A. Balzarotti, Appl. Phys. Lett. **89**, 041904 (2006).

[20] M. Stoffel, G. S. Kar, U. Denker, A. Rastelli, H. Sigg, and O. G. Schmidt, Physica E (Amsterdam) **23**, 421 (2004).

[21] M. Brehm, M. Grydlik, H. Lichtenberger, T. Fromherz, N. Hrauda, W. Jantsch, F. Schäffler, and G. Bauer, Appl. Phys. Lett. **93**, 121901 (2008).

[22] P. Schittenhelm, M. Gail, and G. Abstreiter, J. Cryst. Growth **157**, 260 (1995).

[23] O. G. Schmidt, C. Lange, and K. Eberl, Appl. Phys. Lett. **75**, 1905 (1999).

[24] M. Wachter, F. Schäffler, H. J. Herzog, K. Thonke, and K. Sauer, Appl. Phys. Lett. **63**, 376 (1993).

[25] See EPAPS Document No. E-PRBMDO-80-035944 for extracting single photoluminescence spectra from movie 1. For more information on EPAPS, see http://www.aip.org/pubservs/epaps.html.

[26] V_1 and V_{is} are slightly different, owed to the different relaxation taking place in the island configuration and in the WL. Both volumes can be estimated as $V = V_0(1 + \text{Tr } \varepsilon)$, where ε is the strain tensor (in the island or in the WL) and V_0 is the reference (Ge bulk) volume. While all theoretical results reported in the figures were obtained by considering such correction, for the rather shallow islands here considered we verified that setting $V_1 = V_{is} = V$ is a good approximation. For sake of simplicity, therefore, results are (safely) discussed in terms of a common V value.

[27] Calculations in Ref. 18 are carried out up to $N=5$, showing a tendency toward convergence but not a true limiting value. While in the present paper vales above $N=5$ are not relevant, we have extended our calculations up to $N=6$, imposing full convergence of the surface energy at the $N=5$ value to better emphasize the thick-film limit.

[28] L. G. Wang, P. Kratzer, M. Scheffler, and N. Moll, Phys. Rev. Lett. **82**, 4042 (1999).

[29] P. Kratzer, Q. K. K. Liu, P. Acosta-Diaz, C. Manzano, G. Costantini, R. Songmuang, A. Rastelli, O. G. Schmidt, and K. Kern, Phys. Rev. B **73**, 205347 (2006).

[30] P. Raiteri, D. B. Migas, L. Miglio, A. Rastelli, and H. von Känel, Phys. Rev. Lett. **88**, 256103 (2002).

[31] D. B. Migas, S. Cereda, F. Montalenti, and L. Miglio, Surf. Sci. **556**, 121 (2004).

[32] In our model we simply compare pyramids, domes, and wetting layer. Indefinite dome enlargement in a real system would be opposed by several effects (kinetic limitations, further shape transformation, deep trenches formation and SiGe intermixing, dislocation nucleation, island-island elastic repulsion, etc.) not considered in our treatment, only aimed at understanding the first stages of growth.

[33] I. Daruka and A. L. Barabási, Phys. Rev. Lett. **79**, 3708 (1997).

[34] F. M. Ross, J. Tersoff, and R. M. Tromp, Phys. Rev. Lett. **80**, 984 (1998).

[35] F. Montalenti, P. Raiteri, D. B. Migas, H. von Känel, A. Rastelli, C. Manzano, G. Costantini, U. Denker, O. G. Schmidt, K. Kern, and L. Miglio, Phys. Rev. Lett. **93**, 216102 (2004).

[36] F. M. Ross, R. M. Tromp, and M. C. Reuter, Science **286**, 1931 (1999).

[37] G. Costantini, A. Rastelli, C. Manzano, R. Songmuang, O. G. Schmidt, K. Kern, and H. von Känel, Appl. Phys. Lett. **85**, 5673 (2004).

[38] V. A. Shchukin, E. Schöll, and P. Kratzer, in *Semiconductor Nanostructures*, edited by D. Bimberg (Springer, Berlin, 2008).

[39] G. Kresse and J. Hafner, Phys. Rev. B **47**, 558 (1993).

[40] G. Kresse and J. Hafner, Phys. Rev. B **49**, 14251 (1994).

[41] G. Kresse and J. Furthmüller, Comput. Mater. Sci. **6**, 15 (1996).

[42] G. Kresse and J. Furthmüller, Phys. Rev. B **54**, 11169 (1996).

[43] D. M. Ceperley and B. J. Alder, Phys. Rev. Lett. **45**, 566 (1980).

[44] J. P. Perdew and A. Zunger, Phys. Rev. B **23**, 5048 (1981).

[45] D. Vanderbilt, Phys. Rev. B **41**, 7892 (1990).

[46] G. Kresse and J. Hafner, J. Phys.: Condens. Matter **6**, 8245 (1994).

[47] G. Vastola, F. Montalenti, and L. Miglio, J. Phys.: Condens. Matter **20**, 454217 (2008).

[48] A. A. Stekolnikov and F. Bechstedt, Phys. Rev. B **72**, 125326 (2005).

[49] O. E. Shklyaev, M. J. Beck, M. Asta, M. J. Miksis, and P. W. Voorhees, Phys. Rev. Lett. **94**, 176102 (2005).